Journal of Power Sources 196 (2011) 754–763

Contents lists available at ScienceDirect

Journal of Power Sources

journal homepage: www.elsevier.com/locate/jpowsour

Mechanism for carbon direct electrochemical reactions in a solid oxide electrolyte direct carbon fuel cell

Chen Li, Yixiang Shi, Ningsheng Cai*

Key Laboratory for Thermal Science and Power Engineering of Ministry of Education, Department of Thermal Engineering, Tsinghua University, Beijing 100084, China

ARTICLE INFO

Article history:
Received 28 June 2010
Received in revised form 25 July 2010
Accepted 26 July 2010
Available online 30 July 2010

Keywords:
Mechanism
Electrochemical reaction
Direct carbon fuel cell
Solid oxide
Carbon

ABSTRACT

The carbon direct electrochemical reactions in a solid oxide electrolyte direct carbon fuel cell (DCFC) are investigated experimentally with CH_4-deposited carbon at the anode as fuel. The surface morphology of the anode cross-sections is characterized using a scanning electron microscope (SEM), the elemental distribution using an energy dispersive spectrometer (EDS) and an X-ray photoelectron spectroscopy (XPS), and the deposited carbon microstructures using a Raman spectrometer. The results indicate that all the carbon deposited on the yttrium-stabilized zirconium (YSZ) particle surfaces, the Ni particle surfaces, as well as the three-phase boundary, can participate in the electrochemical reactions during the fuel cell discharging. The direct electrochemical reactions for carbon require the two conditions that the O^{2-} in the ionic conductor contact with a carbon reactive site and that the released electrons are conducted to the external circuit. The electrochemical reactions for the deposited carbon are most difficult on the Ni particle surfaces, easier on the YSZ particle surfaces and easiest at the three-phase boundary. Not all the carbon deposited in the anode participates in the direct electrochemical reactions. The deposited carbon and the O^{2-} in the YSZ react to form the double-bonded adsorbed carbonyl group C═O.

1. Introduction

Fuel cells have been widely recognized as a very efficient and environmentally friendly technology for power generation. The direct carbon fuel cell (DCFC) has a higher theoretical efficiency than other types of fuel cell [1]. In addition, the presence of solid carbon fuel is easily achieved [2] and the DCFC facilitates CO_2 capture. DCFCs can be classified into three types according to the electrolyte used as molten hydroxide [2–6], molten carbonate [7–11] and solid oxide electrolyte [12–19] fuel cells. Some studies have combined molten carbonate and solid oxide electrolytes together [20–22]. The present study focuses on the solid oxide electrolyte DCFC, which has advantages of relatively higher reaction activity because of its higher operating temperatures, and that it may avoid liquid electrolyte consumption, leakage and corrosion.

Existing solid oxide electrolyte DCFCs can be classified into three types according to the type of contact between the anode and the carbonaceous fuel. They may be described as (1) detached [12,13]; (2) physical contact [14,19,23]; and (3) carbon-deposited contact [15–18] type DCFCs. When the anode and carbon fuel are detached, there is no direct electrochemical reaction of the carbon in the DCFC but carbon gasification reactions and gaseous electrochemical reactions occur in the anode. For the physical contact conditions, it is disputed whether direct carbon electrochemical oxidization can occur at the contact interface. Nevertheless, in this situation, the key anode reactions in the DCFC are still the carbon gasification reactions and the electrochemical reactions of the gas species [24]. The rechargeable direct carbon fuel cell (RDCFC) proposed by Ihara et al. [15–18], uses deposited carbon as fuel; it differs from the detached or physical contact designs. The deposited carbon was supplied by thermal decomposition of propane or methane at the anode. The researchers also reported that electrochemical oxidization of carbon occurring during power generation might be described by:

$$C + 2O^{2-} \leftrightarrow CO_2 + 4e^- \quad (1)$$

or

$$C + O^{2-} \leftrightarrow CO + 2e^- \quad (2)$$

When CO is produced, it reacts with O^{2-} so that the DCFC is operated on CO. In this case, the carbon fuel deposited in the porous anode may be in contact with the ionic conductor, the electron conductor or the three-phase boundary. Thus, the carbon-deposited contact-type DCFC may be used for reaction mechanism studies to clarify the actual reaction site (the ionic conductor surface, the electron conductor surface or the three-phase boundary) for carbon electrochemical oxidation.

* Corresponding author. Tel.: +86 10 62789955; fax: +86 10 62789955.
E-mail address: cains@tsinghua.edu.cn (N. Cai).

0378-7753/$ – see front matter © 2010 Elsevier B.V. All rights reserved.
doi:10.1016/j.jpowsour.2010.07.076

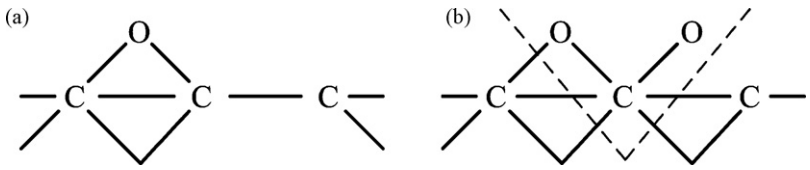

Fig. 1. Pictorial description of the carbon electrochemical oxidation in molten carbonate direct carbon fuel cells [31]: (a) first oxide ion adsorption; (b) second oxide ion adsorption and CO_2 formation.

Ihara et al. [17] suggested that the electrochemical reactions between the deposited carbon and O^{2-} in the ionic conductor could take place only at the three-phase boundary. The released electrons are conducted to the external circuit through the electron conductor Ni. The carbon deposited within the anode but not at the three-phase boundary then takes part in the gasification reaction with CO_2.

Huang et al. [25,26] studied CH_4 carbon deposition in a solid oxide fuel cell (SOFC) and found that the fuel cell could generate electrical current without any gaseous fuel supply. The occurrence of such fuel-free current was thought to be due to the low bulk lattice-oxygen concentration in the anode after oxidation of the deposited carbon, which had extracted some additional lattice oxygen from the anode bulk without replenishment from the cathode. As a result, the carbon deposited on the ionic electron conductor surface could also take part in the direct electrochemical reactions as fuel.

Vayenas et al. [27] reported that the O^{2-} in the anode ionic conductor was electrochemically forced onto the surface of the Ni electron conductor via the polarized metal-electrolyte interfaces, where it released an electron to form O^{-}. Then, the O^{-} at the Ni surface took part in the electrochemical reactions with the gaseous fuel. If this mechanism is reasonable, the deposited carbon, not only at the three-phase boundary, but also at the Ni surface, can take part in the direct electrochemical reactions.

Zhao et al. [28] conducted deposition experiments by separately decomposing methane in a thermo-gravimetric analyzer with Ni, yttrium-stabilized zirconia (YSZ) powders and small chips of anode-supported SOFC button cells as bed materials. They found that the carbon particles deposited in the anode were comparable in size to the Ni and YSZ particles and that the deposited carbon had little opportunity to participate in the electrochemical reactions.

Haupin et al. [29,30] proposed a mechanism for the anodic oxidation of carbon in a molten cryolite/alumina electrolyte. On this basis, Cherepy et al. [31] summarized the mechanism for carbon electrochemical reactions in a molten carbonate electrolyte DCFC as:

$$O^{2-}\ \text{production}: \quad 2{CO_3}^{2-} \rightarrow 2CO_2 + 2O^{2-} \tag{3}$$

$$\text{First}\ O^{2-}\ \text{adsorption}: \quad C_{RS} + O^{2-} \rightarrow C_{RS}O^{2-} \tag{4}$$

$$\text{Fast discharge}: \quad C_{RS}O^{2-} \rightarrow C_{RS}O^{-} + e^{-} \tag{5}$$

$$\text{Fast discharge}: \quad C_{RS}O^{-} \rightarrow C_{RS}O + e^{-} \tag{6}$$

$$\text{Second}\ O^{2-}\ \text{adsorption (RDS)}: \quad C_{RS}O + O^{2-} \rightarrow C_{RS}{O_2}^{2-} \tag{7}$$

$$\text{Fast discharge}: \quad C_{RS}{O_2}^{2-} \rightarrow C_{RS}{O_2}^{-} + e^{-} \tag{8}$$

$$\text{Fast discharge and evolution}: \quad C_{RS}{O_2}^{-} \rightarrow C_{RS}O_2(g) + e^{-} \tag{9}$$

$$\text{Total reaction}: \quad C_{RS} + 2{CO_3}^{2-} \rightarrow 3CO_2 + 4e^{-} \tag{10}$$

At 700 °C, the molten carbonate salts strongly dissociate and yield free oxide ions. A free oxide ion will adsorb at a C_{RS} (a carbon reactive site at an edge, defect, step, or other surface imperfection) and is discharged in two single-electron steps to form a strongly bound C–O–C bridge between reactive carbon atoms on the exposed carbon surface (Fig. 1(a)). The second adsorption of an oxide ion onto the $C_{RS}O$ site requires considerable overpotential and extends the surface species to a C–O–C–O–C bridge carbon oxidation (Fig. 1(b)). Subsequent discharge of this adsorbed species occurs in two single-electron transfers to form the unstable group $C_{RS}O_2$, which is readily desorbed as CO_2. If the $C_{RS}O$ is desorbed before the adsorption of the second oxide ion, then CO is produced by the electrochemical reactions. This phenomenon was observed in some experiments with the CO concentration in production proportional to the cell overpotential and operating temperature [32–34].

Zhang et al. [35] used the Extended Hückel Molecular Orbital (EHMO) and the ab initio method to calculate the total energy and charge distribution for an oxide ion absorbed on different positions of various carbon lattices. They concluded that regardless of which lattice defect model was used, the more probable adsorption mechanism would be the double-bonded structure rather than the

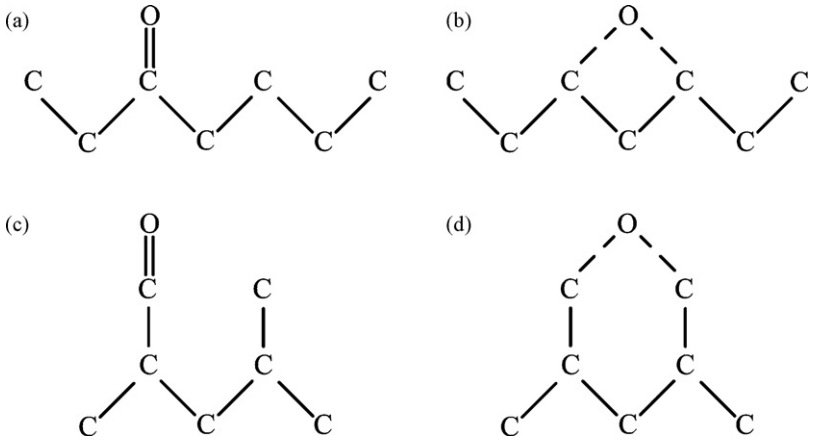

Fig. 2. Surface structure models of oxygen adsorbed on graphite surfaces [35]: (a) double-bonded adsorption with small lattice defects, (b) bridge-type adsorption with small lattice defects, (c) double-bonded adsorption with large lattice defects and (d) bridge-type adsorption with large lattice defects.

Table 1
Experimental procedures for the carbon direct electrochemical reactions.

Cases	Experimental procedures
CH_4 OCV	The button cell circuit was kept open for 30 min using 100 ml min^{-1} CH_4 as the anode gas after being reduced by H_2 and purging by Ar. Then, the anode gas flowrate was changed to 150 ml min^{-1} Ar + 3 ml min^{-1} H_2 and purged for 30 min. While the cell was protected by Ar and H_2, the cell temperature was reduced to ambient temperature at 1.5 °C min^{-1}.
CH_4 0.7V	The button cell was discharged at 0.7 V for 30 min using 100 ml min^{-1} CH_4 as the anode gas after being reduced by H_2 and purged by Ar. Then, the button cell circuit was opened and the anode gas flowrate was changed to 150 ml min^{-1} Ar + 3 ml min^{-1} H_2 and purged for 30 min. Finally, the cell temperature was reduced to ambient temperature at 1.5 °C min^{-1} with the protection of Ar and H_2.
CH_4 DCFC	The button cell was attached to an open circuit for 30 min using 100 ml min^{-1} CH_4 as the anode gas after being reduced by H_2 and purging by Ar. After the carbon deposition by CH_4, the anode gas was switched to 200 ml min^{-1} Ar to purge for 30 min. DCFC discharging: The Ar flowrate was reduced to 20 ml min^{-1} and the button cell was discharged at a constant current density of 300 A m^{-2}. When the cell voltage had decreased to 0 V, the button cell circuit was opened, the anode gas flowrate was switched to 150 ml min^{-1} Ar + 3 ml min^{-1} H_2 and the temperature was reduced to ambient temperature at 1.5 °C min^{-1}.
Control case 1	The button cell circuit was kept open and the anode gas flowrate was set to 150 ml min^{-1} Ar + 3 ml min^{-1} H_2 after being reduced by H_2. Then, the temperature was reduced to ambient temperature at 1.5 °C min^{-1} with the protection of Ar and H_2.
Control case 2	The button cell circuit was kept open with 100 ml min^{-1} O_2 as the anode gas, which made the anode fully oxidized. Then, the anode gas flowrate was switched to 100 ml min^{-1} H_2 to reduce the anode. Finally, the anode gas flowrate was switched to 150 ml min^{-1} Ar + 3 ml min^{-1} H_2 and the temperature was reduced to ambient temperature at 1.5 °C min^{-1}.

bridge-type structure. The corresponding surface structure models for oxygen adsorbed on graphite surfaces are shown in Fig. 2.

However, the mechanisms for carbon direct electrochemical reactions in a solid oxide electrolyte DCFC are quite different from those in a molten carbonate DCFC. Since it is difficult to track the reaction process and to detect the intermediate reaction products, the carbon electrochemical reaction mechanisms have been mainly studied in indirect experiments. Cao et al. [36] assumed that with the oxide ions in the ionic conductor, the electrochemical oxidation of carbon in the solid oxide electrolyte DCFC might follow a similar process to that in molten carbonates. However, there are few studies of the carbon electrochemical reaction mechanisms in solid oxide electrolyte DCFCs, so further research is needed.

This paper describes experiments with a solid oxide electrolyte DCFC with carbon from CH_4 deposited within the anode as fuel. The experiments are carefully designed to analyze the mechanisms for the direct electrochemical reaction of carbon.

2. Experiments

2.1. Anode-supported button cell

An anode-supported SOFC button cell made by SICCAS (Shanghai Institute of Ceramics, Chinese Academy of Sciences) was used in this study. The cell consisted of a Ni/YSZ anode support layer (680 μm), a Ni/scandium-stabilized zirconium (ScSZ) anode active interlayer (15 μm), a ScSZ electrolyte layer (20 μm), and a lanthanum strontium manganate (LSM)/ScSZ cathode layer (15 μm) [24]. The cathode layer was 1.4 cm in diameter and all other layers were 2.6 cm in diameters. Due to relatively simple experimental setups and good repeatability, button cells have been widely used in DCFC experiments [12,15–18]. Our button cells were cut directly from one large cell plate so the anode and electrolyte layers of all cells were fabricated at the same time; thus eliminating the anodic material differences caused by cell to cell variations in fabrication. The test setup provided the experimental conditions for the button cell in the carbon direct electrochemical reaction experiments [37].

2.2. Experimental conditions and procedures

CH_4 was thermally deposited on the cells using three sets of experimental conditions. The mechanisms of carbon direct electrochemical reaction were analyzed based on the characterizations of the deposited anodic carbon for three cases. Two cases without carbon deposition were used as control experiments. During the tests, the temperature of the button cell was maintained at 800 °C and O_2 was used as oxidant at a flow rate of 100 ml min^{-1}. Pure H_2 was fed into the chamber for 1 h at a flow rate of 100 ml min^{-1} to fully reduce the anode. Detailed descriptions of the experimental conditions are given in Table 1.

The cell was cooled down to ambient with Ar (150 ml min^{-1}) and H_2 (3 ml min^{-1}) used as protecting gas. About 2% H_2 was added to maintain a reducing atmosphere in the anode chamber to prevent oxidization of the carbon deposited in the anode.

After the tests, the surface morphology and elemental distribution in the various anode cross-sections were characterized using a scanning electronic microscope (SEM) and an energy dispersive spectrometer (EDS) with an electron probe microanalyzer (JSM-6460, JEOL, Tokyo, Japan). The surfaces of the anode cross-sections were analyzed by an X-ray photoelectron spectroscopy (XPS) (PHI Quantera, ULVAC-PHI, Kanagawa, Japan) with a monochromatic Al Kα ($h\nu$ = 1486.7 eV) X-ray source. To avoid any influence of carbon contamination during the sample transfer and handing, all the sample surfaces were peeled 1.2 nm by an electron gun before characterization. The spot size for analysis was 300 μm × 300 μm. To compensate for the surface-charge effects, the binding energy scale was calibrated with reference to the binding energy of O 1s at 530.2 eV. The survey scans were acquired between 1200 and 0 eV. Concurrent region sweeps for O 1s, Ni 2p, Zr 3d, Y 3d, and C 1s were also obtained. The elemental surface composition was calculated using the transmission values with relative sensitivity factors specific for the instrument equipped with an Al source. The deposited carbon on the anode cross-sections was measured by a Raman Spectrometer (RM2000, Renishaw, New Mills, UK). The excitation line was provided by an Ar^+ laser at 515 nm. The Raman spectra were acquired in the range of 1000–1800 cm^{-1}.

3. Results and discussion

3.1. Characterization of anode elemental distribution

Fig. 3 shows the exterior appearance of the button cells after the tests. The anode surface color represents the degree of carbon deposition. For the CH_4 OCV case, the anode surface color was relatively deep and uniform. Comparison between Fig. 3(a) and (b) shows that the CH_4 DCFC case is relatively lighter in color, especially at the center of the button cell, which indicates that the deposited carbon was consumed during the DCFC discharge process. The decrease of carbon consumption from the cell center to the cell margin is led by the non-uniform current density distribution due to the smaller

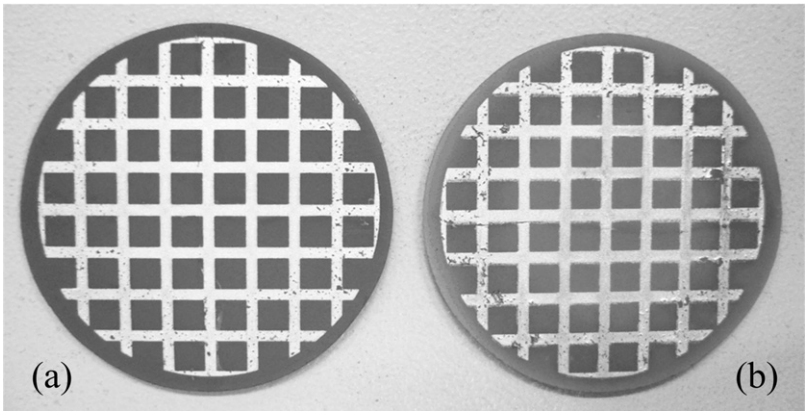

Fig. 3. Exterior anode appearance of button cells after the tests: (a) CH_4 OCV; (b) CH_4 DCFC.

cathode geometry of the cell [38]. The center points were set as the characterization spots.

The elemental analysis results of the anode cross-sections by EDS are listed in Table 2. For the carbon-deposition cases, three points in the anode along the thickness direction were selected as characterization spots: (1) close to the anode outer surface, (2) at the anode center and (3) close to the electrolyte. The anode center for Control case 1 was used as the reference state. All the EDS analyses were performed at 5000 times magnification.

The elemental analysis results for Control case 1 indicate that there is still a little carbon in the anode after the H_2 reduction even without CH_4 cracking. This is because rice starch was used as pore former in the cell fabrication and some residual carbon was not completely oxidized in the cell sintering process. The carbon deposition is most serious in the CH_4 OCV case and is essentially uniformly distributed along the anode thickness direction. However, the carbon atomic percentage for the CH_4 0.7V case is lower than that for the CH_4 OCV case and decreases rapidly from the anode outer surface to the electrolyte layer in the thickness direction. Electrochemical reactions occurred at the anode as the button cell was discharging at a constant voltage with CH_4 as the fuel. The ionic current density would be higher near the electrolyte layer. The results indicate that the polarization potential significantly inhibited the carbon deposition. Compared with the CH_4 OCV case, the DCFC discharging process consumed a large amount of the deposited carbon. It can be deduced that the deposited carbon in the anode was used as fuel for the electrochemical reactions. The carbon atomic percentage on each cross-section was significantly decreased but was still higher than that for Control case 1. The results show that there was still some residual deposited carbon in the anode even when the cell voltage was reduced to 0 V, which indicates that not all the deposited carbon can participate in the direct electrochemical reactions.

Fig. 4 shows the SEM micrographs and surface element distribution maps of the anode cross-sections for the CH_4 OCV case. The four elements C, Ni, O and Zr completely covered the cross-section. In the reduced anode, the O and Zr are mainly in the form of ZrO_2 with Ni in its elemental form. As can be seen from the element distributions, O and Zr have exactly the same shape distribution, covering about half of the picture. The black blank area is Ni and C. Ni and ZrO_2 had basically the same proportions in the cell preparation, but the element distribution area occupied by Ni is much smaller. Thus, the results indicate that the anodic carbon-deposition reactions for the CH_4 decomposition occurred mainly on the Ni surfaces. The deposited carbon covering the Ni surfaces reduces the Ni in this region. In addition, comparison between the carbon distribution map and the SEM micrographs shows that the deposited carbon mostly agglomerated on the Ni surfaces.

Since the error of EDS analysis in the application to the detection of low atomic weight elements (C, O, etc.) is relatively large, the results are usually quasi-quantitative. However, XPS measurements for low atomic weight elements are more accurate. In addition, the large testing spot used in XPS measurements could well reduce the accidental errors caused by test position. Here, XPS was used to further characterize the anodic carbon deposition with the XPS elemental analysis results for the anode cross-sections as listed in Table 3.

The carbon percentages for Control cases 1 and 2 show that the anode carbon content was significantly reduced after being oxidized for 8 h in the pure O_2 atmosphere at high temperature, which further proves that the residual carbon without deposition was introduced by the incompletely oxidized pore starch. In addition,

Table 2
EDS elemental analysis results for anode cross-sections.

Cases	Position	Atomic percentage (at%)				Weight percentage (wt%)			
		C	O	Ni	Zr	C	O	Ni	Zr
CH_4 OCV	Outside	76.25	12.95	6.68	4.12	48.43	10.95	20.73	19.89
	Center	79.40	9.11	7.92	3.56	50.48	7.72	24.62	17.12
	Inside	69.47	15.80	8.55	6.18	38.75	11.74	23.31	26.20
CH_4 0.7V	Outside	61.78	20.40	8.69	9.13	30.77	13.53	21.16	34.53
	Center	48.87	28.52	11.91	10.70	21.59	16.78	25.72	35.91
	Inside	23.99	33.67	27.52	14.81	7.60	14.20	42.60	35.60
CH_4 DCFC	Outside	38.77	28.48	19.56	13.19	14.23	13.92	35.08	36.77
	Center	33.44	32.35	19.96	14.24	11.85	15.27	34.57	38.32
	Inside	30.41	38.05	14.75	16.79	10.83	18.06	25.69	45.42
Control case 1	Center	24.63	39.83	17.82	17.72	8.23	17.72	29.09	44.96

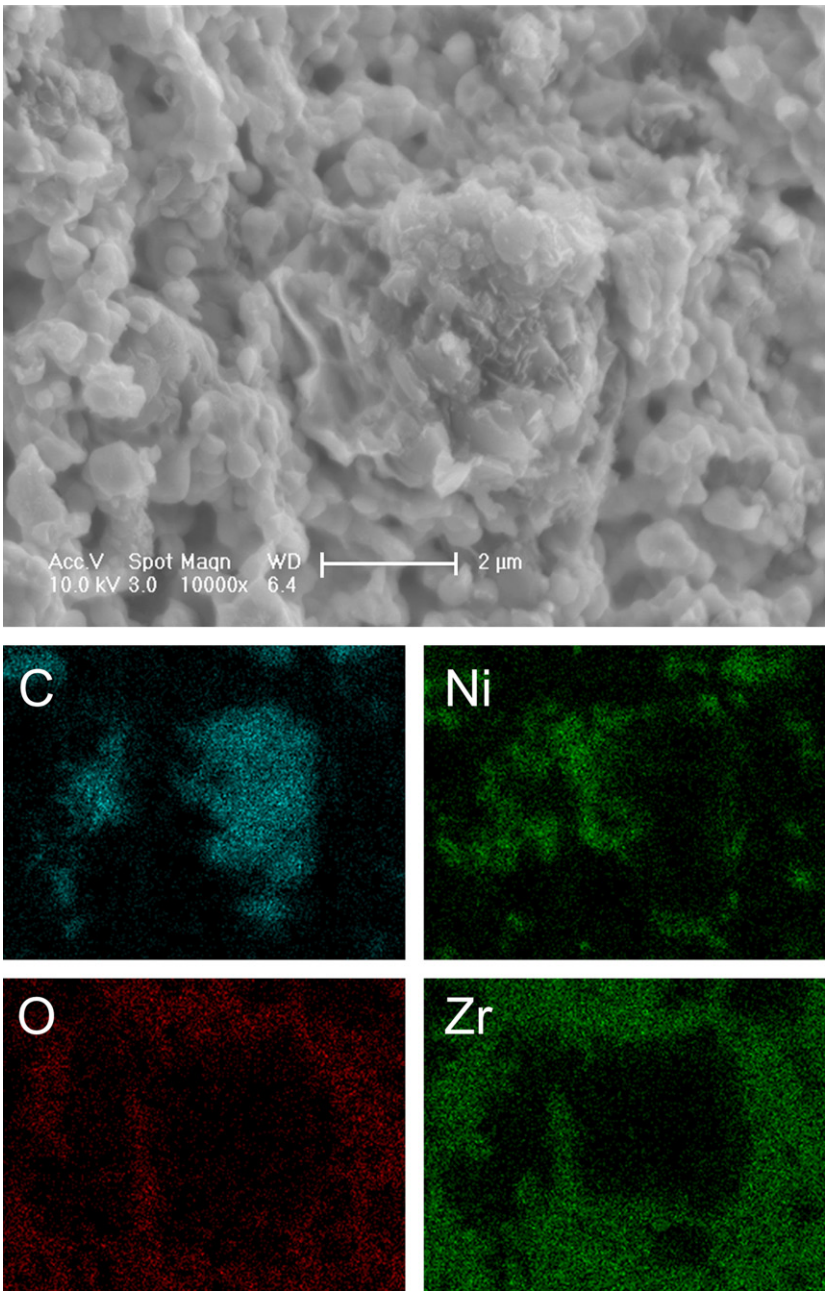

Fig. 4. SEM micrographs and surface element distribution maps of the anode cross-sections for the CH_4 OCV case.

Table 3
XPS elemental analysis results for the anode cross-sections.

Cases	Position	Atomic percentage (at%)				
		C	O	Ni	Zr	Y
CH_4 OCV	Outside	46.05	32.77	9.61	10.05	1.53
	Inside	43.25	35.88	7.74	11.68	1.45
CH_4 0.7V	Outside	26.02	47.89	8.87	15.33	1.89
	Inside	24.90	50.85	8.52	13.80	1.93
CH_4 DCFC	Outside	16.90	47.17	20.33	13.38	2.22
	Inside	15.64	52.24	14.35	15.76	2.02
Control case 1	Center	6.38	58.23	15.01	17.92	2.46
Control case 2	Center	2.60	60.04	15.71	18.75	2.89

the carbon-deposition trends in Table 3 are basically consistent with the EDS results.

The Ni content remained almost unchanged in the CH_4 0.7V case compared to the CH_4 OCV case, while the Zr content increased. The results indicate that there is also a small amount of deposited carbon on the YSZ particle surfaces when the cell was in the open circuit state. In the CH_4 0.7V case, the polarization potential inhibited carbon deposition on the YSZ particle surfaces but had little influence on the deposited carbon on the Ni particle surfaces. The results suggest that the electrochemical reactions took place between the deposited carbon on the YSZ particle surfaces and the O^{2-} conducted in the YSZ when polarized. The emitted electrons from the reactions were conducted to the external circuit through the deposited carbon and the Ni electronic conductor in the anode due to its higher electrical conductivity. Thus, the carbon deposition on the YSZ particle surfaces was inhibited and more O, Zr and Y atoms were exposed. At the same time, the carbon on the Ni particle surfaces had little contact with the O^{2-} conducted in the YSZ and the electrochemical reactions preferentially occurred between the O^{2-} and CH_4. Therefore, the atomic percentage of carbon at any polarization potential was almost the same as that at open circuit. These results further prove that the carbon deposited on the YSZ particle surfaces is more likely to take part in the direct electrochemical reactions than that on the Ni particle surfaces.

Compared with the CH_4 OCV case, the carbon content was reduced while the O, Ni, Zr and Y contents were increased during the DCFC discharging process. This indicates that all the deposited carbon on the YSZ and Ni particle surfaces participated in the electrochemical reactions as the fuel. The O, Zr and Y contents were basically the same as for the CH_4 0.7V case while the Ni content was significantly increased. In this case, the carbon on the Ni particle surfaces was consumed through electrochemical reactions even in the Ar atmosphere.

From above experimental results and mechanistic analysis of the carbon direct electrochemical reactions, it suggests that (1) the deposited carbon at the three-phase boundary and on the surfaces of the YSZ and Ni particles all participate in the electrochemical reactions during the DCFC discharging process; (2) the deposited carbon on the YSZ particle surfaces reacted with the O^{2-} conducted in the YSZ; (3) after all the YSZ particle surface carbon was consumed, the O^{2-} in the YSZ was electrochemically forced onto the Ni surfaces to form O^-. Then, the O^- on the Ni surfaces reacted with the deposited carbon there.

The deposited carbon at the three-phase boundary has the best electrochemical reaction conditions (O^{2-} conducted in the YSZ and e^- conducted in the Ni). In addition, the good electronic conductivity of the carbon means that the carbon deposited on the YSZ particle surfaces is also likely to react with the O^{2-} conducted in the YSZ and e^- conducted in the deposited carbon and Ni. However, the low rate of O^- formation restricts the electrochemical reactions of the carbon deposited on the Ni particle surfaces (O^- formed and diffused on the Ni surface and e^- conducted in the Ni). The experimental results show that there was still some residual deposited carbon in the anode when the cell voltage decreased to 0 V. Thus, the residual deposited carbon could not come into contact with O^- to participate in the reactions. Therefore, the electrochemical reactions of the deposited carbon are most difficult on the Ni particle surfaces, easier on the YSZ particle surfaces and easiest at the three-phase boundary. The ion current density increases with increasing anodic polarization potential, which promotes the direct electrochemical reaction of carbon.

3.2. Raman characterization of deposited carbon in the anode

Raman spectroscopy has been used extensively to characterize the structural features of carbonaceous matters since Tuinstra et al. [39] in 1970 first correlated the Raman bands to structural parameters measured from XRD for polycrystalline graphite. The G (graphite) and D (defect) bands of the Raman spectra are generally used to investigate the carbon structure and to correlate other characteristics. However, Raman spectra cannot give quantitative results for the structural parameters by simply considering the G and D bands, mainly due to the large 'overlap' between these two 'bands'. Structural defects may originate from many structural features in disordered carbon materials. In particular, much structural information can be hidden in the 'overlap' between the G and D bands for highly disordered carbonaceous materials but the G and D bands of highly disordered carbonaceous materials are too broad to have definite meaning. Therefore, deconvolution (curve fits) of the Raman spectra has been used in some studies to acquire more detailed information about the carbon structures [40–42].

Here, the Raman spectra of the deposited carbon on the anode cross-sections were characterized in a range of 1000–1800 cm^{-1} and deconvoluted using six bands according to the present experimental results and studies in the literature. For highly disordered carbonaceous materials, the G band at 1580–1600 cm^{-1} [40] and the D band at 1335–1355 cm^{-1} [42] are usually referred to as the Graphite and Defect bands. Here, the G band from the deconvolution results showed two peaks, assigned as G_1 and G_2. Li et al. [40] pointed out a G_R band at 1540 cm^{-1}, which represents aromatic structures with 3–5 rings in amorphous carbon materials. The G_L band at 1700 cm^{-1} represents the carbonyl group C=O [43] with slight differences in the G_L band for different carbonaceous materials. The G_L band has been known to have two peaks at 1680 and 1745 cm^{-1} [44,45], which is consistent with the present experiment results. These were assigned as G_{L1} and G_{L2}. The assignments of the six bands are summarized in Table 4.

As indicated in Section 3.1, there was residual carbon in the anode introduced by the incompletely oxidized pore starch. Fig. 5 shows the Raman spectra for anode cross-sections for the control cases. There are no obvious peaks in the Raman spectra besides the measurement noise. Therefore, the influence of the residual carbon from the cell preparation was negligible for the carbon Raman spectra analysis.

The Raman spectra of the deposited carbon in the range of 800 and 1800 cm^{-1} were deconvoluted using these bands with six pure Gaussian peaks using the Peakfit software. During the curve fitting, the band positions were fixed while the bandwidths were

Table 4
Raman band assignment summary for the anodic deposited carbon.

Band name	Band position (cm^{-1})	Band type	Description
D	1350	sp^2	Highly disordered carbonaceous materials; C–C bonds between aromatic rings and aromatics with no less than 6 rings
G_R	1540	sp^2	Aromatics with 3–5 rings; amorphous carbon structures
G_1	1583	sp^2	Graphite; alkene C=C
G_2	1600	sp^2	
G_{L1}	1680	sp^2	Carbonyl group C=O
G_{L2}	1741	sp^2	

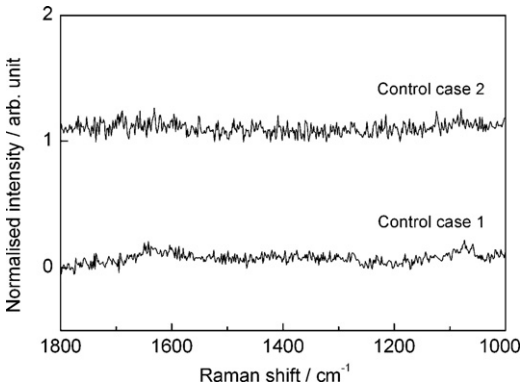

Fig. 5. Raman spectra for the anode cross-sections for the control cases.

restrained to the same maximum limits. Fig. 6 shows the Raman spectra deconvolution results for the anodic deposited carbon for various conditions.

The ratio (I_D/I_G) of the D band to G band intensities (peak areas) in the Raman spectrum deconvolution has been extensively used as an important parameter to study crystalline or graphite-like carbon structures. Some researchers have correlated the I_D/I_G ratio with the average in-plane length of carbon crystallite structures [39,46–48]. A decrease in the I_D/I_G ratio is normally expected with increasing graphitization. Other ratios of band intensity have also been used often. Here, three band intensity ratios, I_D/I_G, I_{GR}/I_G and I_{GL}/I_G, were used to analyze the Raman spectra. The Raman spectra deconvolution data for anodic deposited carbon is listed in Table 5.

The anodic deposited carbon typical contains disordered carbon, graphite and the carbonyl group C=O. The anode chamber was always maintained in a strong reducing atmosphere for the carbon-deposition cases with no O in the anodic gas. Thus, the existence of the carbonyl group C=O indicates that the direct electrochemical reaction occurred between the O^{2-} in the YSZ and the deposited carbon in the anode to form the double-bonded adsorbed carbonyl group C=O.

The I_D/I_G for the CH_4 0.7V case is larger than for the CH_4 OCV case which indicates that the disordered carbon content increased and the graphite content decreased at the given polarization potential. At the same time, I_{GL}/I_G increased as more O was adsorbed on the deposited carbon and formed more carbonyl groups, C=O. Thus, the polarization potential can enhance the direct electrochemical reactions of carbon.

During the DCFC discharge process, the carbonyl group C=O was continuously consumed to form CO or CO_2 when combined with another O, while the O^{2-} in YSZ took part in the direct electrochemical reactions and formed new carbonyl groups, C=O. When the cell voltage decreased to 0 V, the residual anodic deposited carbon could not react with O^{2-} and the carbonyl group, C=O, content

Table 5
Raman spectra deconvolution data of anodic deposited carbon.

Band information		Experiment cases		
Band name	Band position (cm^{-1})	CH_4 OCV	CH_4 0.7V	CH_4 DCFC
D	1350	27.93	27.65	33.26
G_R	1540	6.61	5.49	6.00
G_1	1583	23.35	18.07	23.53
G_2	1600	22.08	26.01	22.22
G_{L1}	1680	12.72	14.87	9.82
G_{L2}	1741	7.31	7.91	5.16
	I_D/I_G	0.615	0.627	0.727
	I_{GR}/I_G	0.145	0.125	0.131
	I_{GL}/I_G	0.441	0.517	0.328

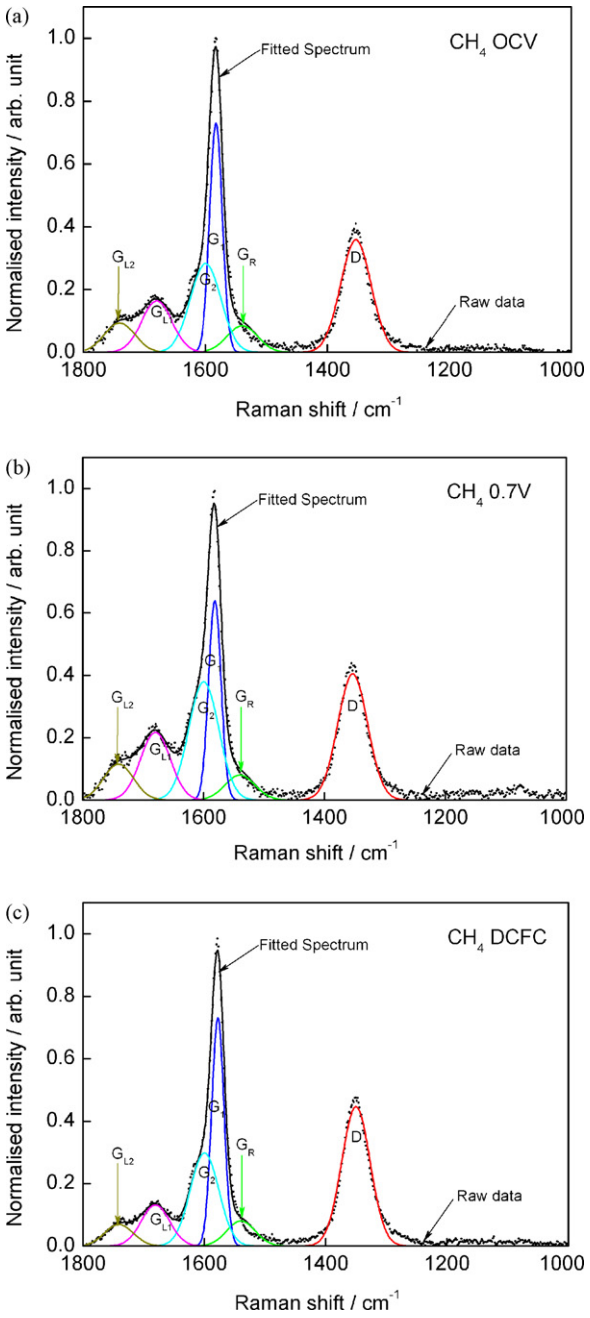

Fig. 6. Raman spectra deconvolutions of anodic deposited carbon for various conditions: (a) CH_4 OCV, (b) CH_4 0.7V and (c) CH_4 DCFC.

decreased. Therefore, I_{GL}/I_G for the CH_4 DCFC case was smaller than without discharging (the CH_4 OCV case). In addition, the increased I_D/I_G after discharging indicates that the graphite in the deposited carbon also reacted with the O^{2-}. Thus, the graphite structure was destroyed, defects appeared and the graphite content decreased.

3.3. XPS characterization of the anode cross-sections

XPS was used to characterize the near-surface element states in the anode cross-sections after the tests. The XPS surface spectra for O, Ni, Zr and Y are shown in Fig. 7. Control case 2 is given as the control data for the XPS spectra for the anode without carbon deposition. The binding energy for O was near 530.2 eV, which corresponds to the O 1s orbital of ZrO_2. The O 1s peak of the carbonyl group C=O was not detected in Fig. 7(a) because the carbonyl group

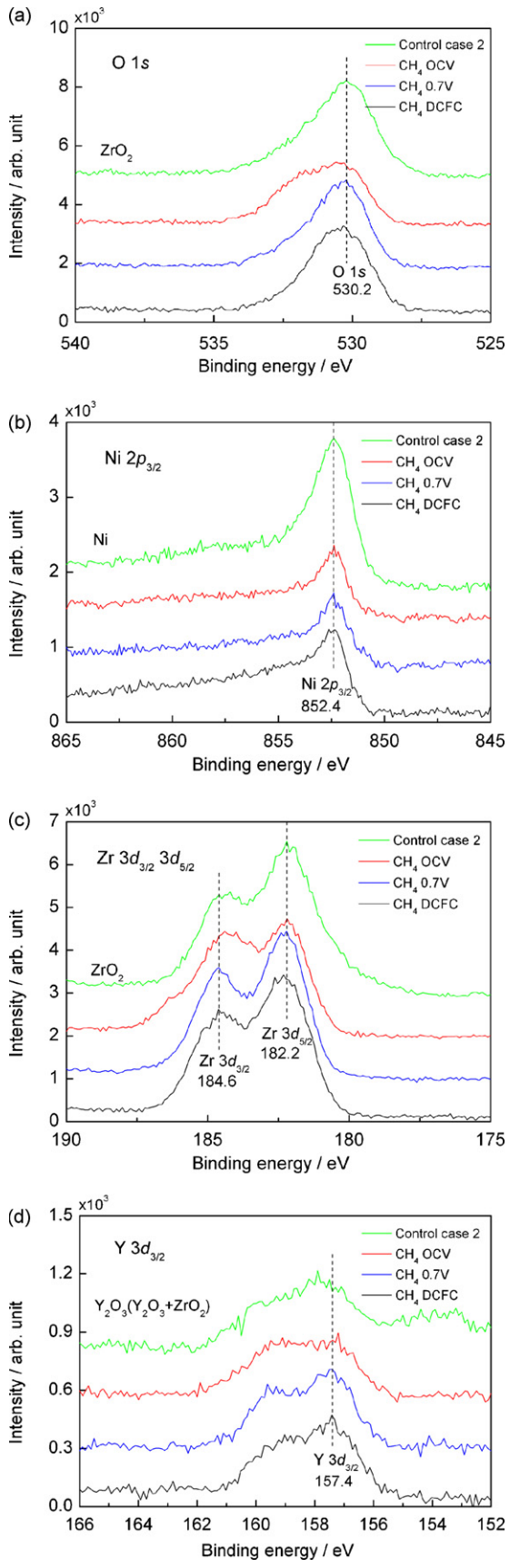

Fig. 7. XPS spectra for (a) O 1s, (b) Ni $2p_{3/2}$, (c) Zr $3d_{3/2}$, $3d_{5/2}$ and (d) Y $3d_{3/2}$.

Table 6
Deconvolution results of the C 1s XPS spectra for various conditions.

Cases	C 1s deconvolution results				
	Formation	Binding energy (eV)	Half peak width (eV)	Area	Percentage (%)
Base case 2	C/Ni (284.7 eV)	284.98	3.04	794.8	100
CH_4 OCV	C/Ni (284.7 eV)	284.84	1.48	3675.4	85.5
	C=O (≈286.3 eV)	286.59	1.48	624.7	14.5
CH_4 0.7V	C/Ni (284.7 eV)	284.33	1.63	1047.1	49.8
	C=O (≈286.3 eV)	286.16	1.63	1055.0	50.2
CH_4 DCFC	C/Ni (284.7 eV)	284.60	2.46	1575.0	100

C=O content was relatively small near the surface and the corresponding binding energy (530.1 eV) was very close to that of ZrO_2. The peak for Ni $2p_{3/2}$ was observed at a binding energy of 852.4 eV indicating that Ni was in its elemental form after H_2 reduction. The comparisons in Fig. 7(b) show that Control case 2 had the largest Ni $2p_{3/2}$ peak area because the carbon deposited on the Ni surface was reduced and more Ni surface was exposed, which is consistent with the SEM and EDS results. As shown in Fig. 7(c), the XPS spectra for Zr 3d contained a doublet at binding energies of 184.6 and 182.2 eV, which can be assigned as the Zr $3d_{5/2}$ and Zr $3d_{3/2}$ lines. In addition, the Y $3d_{3/2}$ peak in Fig. 7(d) is near 157.4 eV, which is in good agreement with the standard peak for the YSZ ($Y_2O_3 + ZrO_2$) anode material.

The carbon on the anode cross-section was the focus of the XPS characterization. The C 1s XPS peak was deconvoluted using pure Gaussian peaks with the same maximum bandwidths for each given case. Fig. 8 shows the deconvolution of the C 1s XPS spectra for various conditions.

In the standard carbon spectra, the binding energy of C 1s for carbon deposited on a Ni surface, C/Ni, is 284.7 eV while the binding energy of C 1s in the carbonyl group C=O in most materials is about 286.3 eV. In Control case 2, the peak for C 1s was observed at 284.98 eV. The noise ratio in the spectrogram is relatively large due to the low carbon content. Fig. 8(b) shows the presence of C/Ni and C=O by the major peak at 284.84 eV and the minor peak at 286.59 eV. The results indicate that the carbon is deposited mainly on the Ni surface with a small part of the deposited carbon reacted with O^{2-} to form C=O. As shown in Fig. 8(c), after the carbon deposition from CH_4 during the 0.7 V discharging for 30 min, the XPS spectra for C 1s showed significant double peaks (at 284.33 and 286.16 eV) corresponding to C/Ni and C=O. The peak at 288.24 eV was within the curve fit accuracy and could be treated as a fitting error. The C=O peak area increased from 14.5% for the CH_4 OCV case to 50.2% for the CH_4 0.7V case. Therefore, the polarization promotes the direct electrochemical reactions of carbon and the formation of C=O. The C 1s XPS spectra for the CH_4 DCFC case before constant current discharging should be the same as for the CH_4 OCV case. However, only the C/Ni peak was observed with a binding energy of 284.60 eV after the discharging, as shown in Fig. 8(d). The direct electrochemical reactions of carbon are assumed to have occurred during the DCFC discharging with the carbonyl group C=O continuously consumed to form CO or CO_2 with another O. Thus, the C=O peak was not detected after the tests.

The deconvolution results for the C 1s XPS spectra for various conditions are listed in Table 6. The half peak width represents the intensity of the carbon excitation. A small half peak width indicates high excitation intensity and large carbon content. The half peak widths in Table 6 show that the carbon contents on the anode cross-sections for various cases decreased in order of CH_4 OCV > CH_4 0.7V > CH_4 DCFC > Control case 2, which is consistent with the results in Section 3.1.

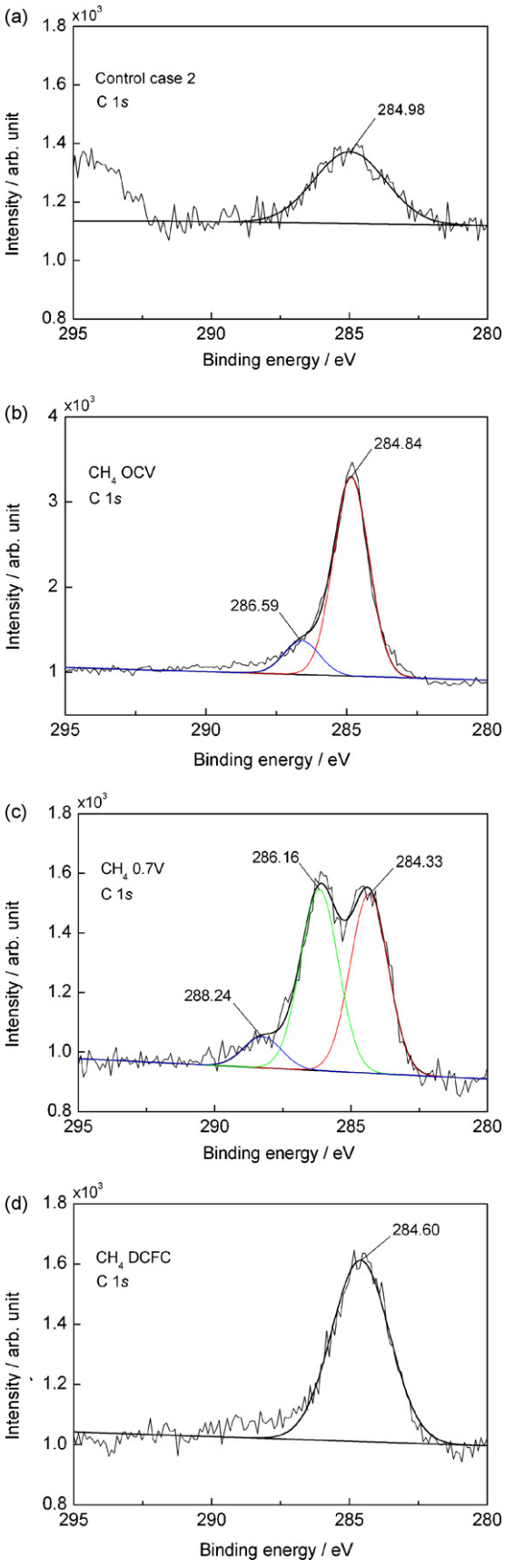

Fig. 8. Deconvolution of C 1s XPS spectra for various conditions: (a) control case 2, (b) CH_4 OCV, (c) CH_4 0.7V and (d) CH_4 DCFC.

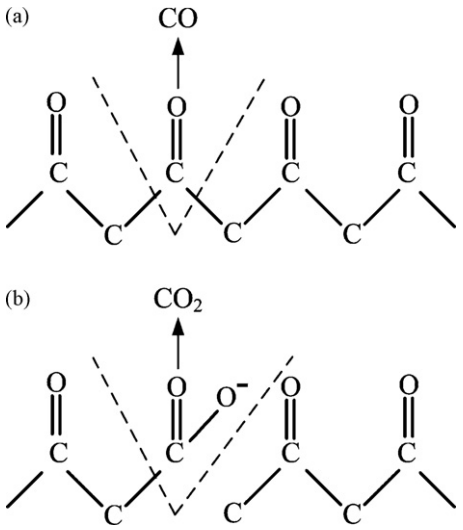

Fig. 9. Pictorial description of the carbon direct electrochemical oxidation in solid oxide direct carbon fuel cells: (a) first oxide ion adsorption and CO formation; (b) second oxide ion adsorption and CO_2 formation.

3.4. Mechanism for the carbon direct electrochemical reactions

From above experimental results and mechanism analysis, a mechanism for the carbon direct electrochemical reactions in solid oxide electrolyte DCFC anode is proposed as:

$$O^{2-}\ \text{production}: \quad O_O^x \rightarrow O^{2-} + V_O^{\cdot\cdot} \tag{11}$$

$$\text{First}\ O^{2-}\ \text{adsorption}: \quad C_{RS} + O^{2-} \rightarrow C_{RS}O^{2-} \tag{12}$$

$$\text{Fast discharge}: \quad C_{RS}O^{2-} \rightarrow C_{RS}O^{-} + e^{-} \tag{13}$$

$$\text{Fast discharge}: \quad C_{RS}O^{-} \rightarrow C_{RS}O + e^{-} \tag{14}$$

$$\text{CO desorption}: \quad C_{RS}O \rightarrow CO(g) \tag{15}$$

$$\text{Second}\ O^{2-}\ \text{adsorption}: \quad C_{RS}O + O^{2-} \rightarrow C_{RS}O_2{}^{2-} \tag{16}$$

$$\text{Fast discharge}: \quad C_{RS}O_2{}^{2-} \rightarrow C_{RS}O_2{}^{-} + e^{-} \tag{17}$$

$$\text{Fast discharge and } CO_2 \text{ desorption}: \quad C_{RS}O_2{}^{-} \rightarrow C_{RS}O_2(g) + e^{-} \tag{18}$$

$$\text{Total reaction}: \quad \begin{matrix} C_{RS} + O^{2-} \rightarrow CO + 2e^{-} \\ C_{RS} + 2O^{2-} \rightarrow CO_2 + 4e^{-} \end{matrix} \tag{19}$$

During the DCFC discharging, the O^{2-} is conducted into the anode ionic conductor YSZ. An O^{2-} reacts with a carbon reactive site, C_{RS}, of the deposited carbon in the anode and is discharged in two single-electron steps to form a double-bonded adsorbed structure $C_{RS}O$ (carbonyl group C=O, including adsorption with small and large lattice defects). Then, the $C_{RS}O$ is desorbed as CO or absorbs a second O^{2-} to produce CO_2 in a subsequent single-electron transfer. The total reactions in the solid oxide electrolyte DCFC are given by Eq. (19). Fig. 9 illustrates the carbon direct electrochemical oxidation in solid oxide direct carbon fuel cells.

4. Conclusions

Experiments were conducted to analyze the carbon direct electrochemical reaction mechanisms in a solid oxide electrolyte DCFC. A mechanism for the carbon direct electrochemical reactions in solid oxide electrolyte DCFC anode is proposed Unlike the molten carbonate DCFC, the direct electrochemical reactions of carbon in

the solid oxide electrolyte DCFC are closely related to the positions of the deposited carbon with the following features:

1. The direct electrochemical reactions of carbon require that the O^{2-} in the anode ionic conductor contact with a carbon reactive site and the released electron conduct to the external circuit.
2. Carbon deposition in the anode mainly occurs on the Ni surfaces as superficial agglomerates. There is also some deposited carbon on the ionic conductor YSZ surface. During the DCFC discharge process, all the deposited carbon at the three-phase boundary and the YSZ and Ni particle surfaces can participate in the electrochemical reactions but the reaction paths are slightly different.
3. The deposited carbon at the three-phase boundary reacts with the O^{2-} conducted in the YSZ and the released e^- conducted through the Ni particles to the external circuit. Similarly, owing to the good electronic conductivity of the carbon, the deposited carbon on the YSZ surfaces also reacts with the O^{2-} conducted in the YSZ with the released e^- conducted through the deposited carbon and the Ni to the external circuit. However, for carbon deposited on the Ni surfaces, the O^{2-} in the YSZ is electrochemically forced onto the Ni surface where it forms O^- which then reacts with the carbon deposited on the Ni surface with the released e^- conducted through the Ni particles to the external circuit.
4. The electrochemical reactions of the deposited carbon are most difficult on the Ni particle surfaces, easier on the YSZ particle surfaces and easiest at the three-phase boundary. Not all of the deposited carbon participates in the direct electrochemical reactions.
5. The carbon deposited in the anode and the O^{2-} in the YSZ react to form a double-bonded adsorbed carbonyl group C═O, adsorption structure (including adsorption with small and large lattice defects).
6. The polarization promotes the direct electrochemical reactions of carbon and the C═O formation.

Acknowledgements

This work was supported by the National Natural Science Foundation of China (20776078) and the Chinese High Technology Development Project (2007AA05Z151). We gratefully acknowledge the insightful discussions and the button cells used in experiments produced by Prof. Shaorong Wang of the Shanghai Institute of Ceramics Chinese Academy of Sciences (SICCAS), China. We also thank Prof. David Christopher for editing the English.

References

[1] S. Basu, Recent Trends in Fuel Cell Science and Technology, Anamaya, New Delhi, 2007.
[2] S. Zecevic, E.M. Patton, P. Parhami, Carbon 42 (2004) 1983–1993.
[3] T.A. Edison, US 460122 (1891).
[4] W.W. Jacques, US 555511 (1896).
[5] G.A. Hackett, J.W. Zondlo, R. Svensson, J. Power Sources 168 (2007) 111–118.
[6] T. Nunoura, K. Dowaki, C. Fushimi, S. Allen, E. Meszaros, M.J. Antal, Ind. Eng. Chem. Res. 46 (2007) 734–744.
[7] W.H.A. Peelen, M. Olivry, S.F. Au, J.D. Fehribach, K. Hemmes, J. Appl. Electrochem. 30 (2000) 1389–1395.
[8] X. Li, Z. Zhu, J. Chen, R. de Marco, A. Dicks, J. Bradley, G. Lu, J. Power Sources 186 (2009) 1–9.
[9] J.R. Selman, J. Power Sources 160 (2006) 852–857.
[10] M. Steinberg, Int. J. Hydrogen Energy 31 (2006) 405–411.
[11] J.F. Cooper, R. Krueger, N. Cherepy, US 6815105 B2 (2004).
[12] N. Nakagawa, M. Ishida, Ind. Eng. Chem. Res. 27 (1988) 1181–1185.
[13] T.M. Gür, R.A. Huggins, J. Electrochem. Soc. 139 (1992) L95–L97.
[14] R. Liu, C. Zhao, J. Li, F. Zeng, S. Wang, T. Wen, Z. Wen, J. Power Sources 195 (2010) 480–482.
[15] M. Ihara, K. Matsuda, H. Sato, C. Yokoyama, Solid State Ionics 175 (2004) 51–54.
[16] M. Ihara, S. Hasegawa, J. Electrochem. Soc. 153 (2006) A1544–A1546.
[17] S. Hasegawa, M. Ihara, J. Electrochem. Soc. 155 (2008) B58–B63.
[18] H. Saito, S. Hasegawa, M. Ihara, J. Electrochem. Soc. 155 (2008) B443–B447.
[19] S. Li, A.C. Lee, R.E. Mitchell, T.M. Gür, Solid State Ionics 179 (2008) 1549–1552.
[20] S.L. Jain, Y. Nabae, B.J. Lakeman, K.D. Pointon, J.T.S. Irvine, Solid State Ionics 179 (2008) 1417–1421.
[21] K. Pointon, B. Lakeman, J. Irvine, J. Bradley, S. Jain, J. Power Sources 162 (2006) 750–756.
[22] A.S. Lipilin, I.I. Balachov, L.H. Dubois, A. Sanjurjo, M.C. McKubre, S. Crouch-Baker, M.D. Hornbostel, F.L. Tanzclla, US 0269688 A1 (2007).
[23] S.S.C. Chuang, Carbon-Based Fuel Cell, University of Akron, USA, 2006.
[24] C. Li, Y. Shi, N. Cai, J. Power Sources 195 (2010) 4660–4666.
[25] T. Huang, C. Wang, Chem. Eng. J. 132 (2007) 97–103.
[26] T. Huang, M. Huang, J. Power Sources 168 (2007) 229–235.
[27] C.G. Vayenas, S. Bebelis, S. Neophytides, I.V. Yentekakis, Appl. Phys. A: Mater. Sci. Process. 49 (1989) 95–103.
[28] X.Y. Zhao, Q. Yao, S.Q. Li, N.S. Cai, J. Power Sources 185 (2008) 104–111.
[29] W.E. Haupin, W.B. Frank, in: J.O.M. Bockris, B.E. Conway, E. Yeager, R.E. White (Eds.), Comprehensive Treatise of Electrochemistry, Electrochemical Processing, vol. 2, Plenum Press, New York, 1981, pp. 301–305.
[30] W.B. Frank, W.E. Haupin, Ullmann's Encyclopedia of Industrial Chemistry, vol. A1, Wiley-VCH, Deerfield Beach, 1985.
[31] N.J. Cherepy, R. Krueger, K.J. Fiet, A.F. Jankowski, J.F. Cooper, J. Electrochem. Soc. 152 (2005) A80–A87.
[32] R.D. Weaver, S.C. Leach, A.E. Bayce, L. Nanis, Direct Electrochemical Generation of Electricity From Coal, SRI International Corp., 1979.
[33] R.D. Weaver, S.C. Leach, L. Nanis, Proceedings of the Intersociety Energy Conversion Engineering Conference, Atlanta, USA, 1981, pp. 717–721.
[34] D.G. Vutetakis, D.R. Skidmore, H.J. Byker, J. Electrochem. Soc. 134 (1987) 3027–3035.
[35] M. Zhang, Y. Zhai, Z. Qiu, H. Liu, N. Chen, Chin. J. Met. Sci. Technol. 7 (1991) 1–8.
[36] D. Cao, Y. Sun, G. Wang, J. Power Sources 167 (2007) 250–257.
[37] C. Li, Y. Shi, N. Cai, J. Power Sources 195 (2010) 2266–2282.
[38] Y. Shi, N. Cai, C. Li, C. Bao, E. Croiset, J. Qian, Q. Hu, S. Wang, J. Power Sources 172 (2007) 246–252.
[39] F. Tuinstra, J.L. Koenig, J. Chem. Phys. 53 (1970) 1126–1130.
[40] X. Li, J. Hayashi, C. Li, Fuel 85 (2006) 1700–1707.
[41] X. Zhu, C. Sheng, Fuel Process. Technol. 91 (2010) 837–842.
[42] N. Larouche, B.L. Stansfield, Carbon 48 (2010) 620–629.
[43] D. Lin-Vien, N.B. Colthup, W.G. Fateley, J.G. Grasselli, The Handbook of Infrared and Raman Characteristic Frequencies of Organic Molecules, Academic Press, San Diego, 1991.
[44] B. Schrader, Raman/Infrared Atlas of Organic Compounds, VCH, Weinheim, Germany, 1989.
[45] R. Singh, Electrochemical and partial oxidation of CH_4, PhD Thesis, University of Akron, USA, 2008.
[46] G.A. Zickler, B. Smarsly, N. Gierlinger, H. Peterlik, O. Paris, Carbon 44 (2006) 3239–3246.
[47] T. Jawhari, A. Roid, J. Casado, Carbon 33 (1995) 1561–1565.
[48] L.G. Cançado, K. Takai, T. Enoki, M. Endo, Y.A. Kim, H. Mizusaki, A. Jorio, L.N. Coelho, R. Magalhães-Paniago, M.A. Pimenta, Appl. Phys. Lett. 88 (2006) 163106.